

Spinel oxides: $\Delta 1$ spin-filter barrier for a class of magnetic tunnel junctions

Jia Zhang, X.-G. Zhang, and X. F. Han

Citation: *Appl. Phys. Lett.* **100**, 222401 (2012); doi: 10.1063/1.4722804

View online: <http://dx.doi.org/10.1063/1.4722804>

View Table of Contents: <http://apl.aip.org/resource/1/APPLAB/v100/i22>

Published by the American Institute of Physics.

Related Articles

Utility of reactively sputtered CuNx films in spintronics devices

J. Appl. Phys. **111**, 073912 (2012)

Probing the oxygen vacancy distribution in resistive switching Fe-SrTiO₃ metal-insulator-metal-structures by micro-x ray absorption near-edge structure

J. Appl. Phys. **111**, 076101 (2012)

Effect of TaOx thickness on the resistive switching of Ta/Pr_{0.7}Ca_{0.3}MnO₃/Pt films

Appl. Phys. Lett. **100**, 143506 (2012)

Low leakage current in metal-insulator-metal capacitors of structural Al₂O₃/TiO₂/Al₂O₃ dielectrics

Appl. Phys. Lett. **100**, 081101 (2012)

Suppression of dielectric crystallization on metal by introduction of SiO₂ layer for metal floating gate memory blocking oxide

Appl. Phys. Lett. **99**, 222903 (2011)

Additional information on Appl. Phys. Lett.

Journal Homepage: <http://apl.aip.org/>

Journal Information: http://apl.aip.org/about/about_the_journal

Top downloads: http://apl.aip.org/features/most_downloaded

Information for Authors: <http://apl.aip.org/authors>

ADVERTISEMENT



Goodfellow
metals • ceramics • polymers • composites
70,000 products
450 different materials
small quantities fast

www.goodfellowusa.com

Spinel oxides: Δ_1 spin-filter barrier for a class of magnetic tunnel junctions

Jia Zhang,^{1,a)} X.-G. Zhang,^{2,b)} and X. F. Han^{1,c)}

¹Beijing National Laboratory for Condensed Matter Physics, Institute of Physics, Chinese Academy of Sciences, Beijing 100190, China

²Center for Nanophase Materials Sciences and Computer Science and Mathematics Division, Oak Ridge National Laboratory, Oak Ridge, Tennessee 37831-6493, USA

(Received 12 April 2012; accepted 13 May 2012; published online 29 May 2012)

The orbital composition of the electrode wave functions and the complex bands within the barrier band gap are two important factors in deciding the spin-filter effect. This is illustrated in a class of spinel oxides, including MgAl_2O_4 , ZnAl_2O_4 , SiMg_2O_4 , and SiZn_2O_4 . Through first-principles calculations of the complex bands and electron transmission along the [001] direction, they are shown to have the same Δ_1 spin-filter effect as MgO due to the combination of both factors. Due to better lattice match with typical bcc magnetic electrodes than MgO , these materials provide a broad spectrum of candidate materials for magnetic tunnel junctions. © 2012 American Institute of Physics. [<http://dx.doi.org/10.1063/1.4722804>]

In magnetic tunnel junctions (MTJs), the lattice structure of the tunnel barrier is a crucial factor for achieving high tunneling magneto-resistance (TMR). The TMR of samples using amorphous alumina barrier^{1,2} can only reach tens of percent. Crystalline MgO barrier, however, was predicted to produce TMR of thousands of percent,^{3,4} and transport properties can be tailored by various metallic insertion layers.⁵⁻⁷ Experimental research^{8,9} in fabricating the MgO based junctions marked a breakthrough in spintronics,¹⁰ and the highest TMR now exceeds 600%.¹¹ This giant TMR is understood to arise from the Δ_1 spin-filter effect of the MgO barrier. The electron with Δ_1 symmetry in magnetic electrodes has the largest transmission when the two magnetic electrodes are in parallel alignment while nearly no transmission when they are in anti-parallel alignment due to the absence of the Δ_1 state in the minority spin channel of the electrodes.

A major drawback of using MgO as the barrier material is the significant strain between the MgO layer and the Fe or FeCo electrode layers, where the lattice mismatch between the two is greater than 3%. This mismatch leads to interface dislocations and barrier defects, which in turn lead to large asymmetry in the junction, rapid reduction of the TMR with the bias voltage, and a low breakdown voltage. The defect due to the large strain is also believed to be one of the factors limiting the improvement of TMR and the origin of electric noise.¹² Alternative barrier materials such as $\text{SrTiO}_3(001)$ and $\text{ZnSe}(001)$ have been attempted, but these yielded very low TMR in experiments.¹⁰ Recently, single crystalline Fe/ MgAl_2O_4 /Fe MTJs have been fabricated, and over 100% TMR ratio was achieved.^{13,14} More importantly, these junctions produced larger V_{half} (bias voltage at which the TMR ratio is half of that at zero-bias) than MgO -based MTJs.¹³ The better bias performance was attributed to the nearly perfect lattice match between Fe and MgAl_2O_4 , whose lattice rotated 45° produces a less than 1% mismatch with Fe. This preliminary experiment suggests that MgAl_2O_4 may be a possible

promising candidate for tunnel barrier in MTJs. However, the question remains on whether MgAl_2O_4 is a Δ_1 spin-filter barrier. Furthermore, other spinel¹⁵ materials also have the nearly perfect lattice match with typical bcc magnetic electrodes. Are these materials also Δ_1 spin-filter barriers?

Traditionally, the spin-filtering ability of a barrier material has been studied by calculating its complex band structure along the direction of transport. Such work has been carried out for MgO ,³ for GaAs and ZnSe,¹⁷ and for insulator Kotoite $\text{Mg}_3\text{B}_2\text{O}_6$,²³ all of which have been shown to be Δ_1 spin-filter barriers. However, the spinel oxides are different. They have the C_{2v} symmetry along the [001] direction. The bands along this direction are the $\tilde{\Delta}_1$, $\tilde{\Delta}_2$, $\tilde{\Delta}_3$, and $\tilde{\Delta}_4$ bands. They do not have an one-to-one correspondence to the Δ_1 , Δ_2 , Δ_2' , and Δ_5 bands defined by the C_{4v} symmetry of the bcc electrodes. In particular, the symmetry of the slowest decaying complex band in the spinel oxides, $\tilde{\Delta}_1$ band, matches to both Δ_1 and Δ_2' bands in the electrodes. Thus the complex band calculation alone will not be able to determine the spin-filter property of the spinel oxides.

In this letter, the complex band and the transmission probability along the [001] direction for spinel oxides MgAl_2O_4 , ZnAl_2O_4 , SiMg_2O_4 and SiZn_2O_4 are studied. We show that the $\tilde{\Delta}_1$ complex band has the slowest decay rate in these materials. Although both Δ_1 and Δ_2' Fe bands match the $\tilde{\Delta}_1$ complex band in the spinel oxides, only the Δ_1 state has a significant transmission, whereas the Δ_2' electron wave function decays very fast in the barrier layer. This difference is attributed to the difference in the orbital composition of the two Bloch states.³ The spin-filter effect and good lattice match will make the spinel oxides ideal candidate materials for barriers in MTJs.

All the calculations are performed by using pseudopotential plane wave and the local density approximation of the density functional theory as implemented in Quantum Espresso package.^{18,19} A 60 Ryd cutoff energy and $8 \times 8 \times 8$ Monkhorst-Pack k-point grids²⁰ are used, which are sufficient to converge the total energy. Normal AB_2O_4 spinel structure has space group $\text{Fd}\bar{3}m$. As shown in Fig. 1(a), the conventional unit cell of spinel oxides contains 56 atoms.

^{a)}Electronic mail: zhangjia@iphy.ac.cn.

^{b)}Electronic mail: xgz@ornl.gov.

^{c)}Electronic mail: xfhan@aphy.iphy.ac.cn.

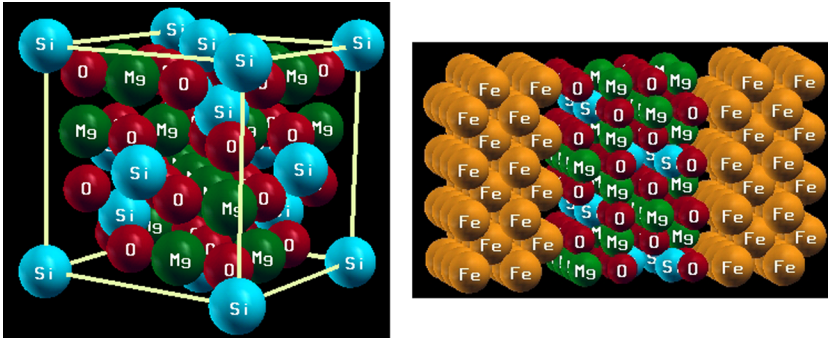


FIG. 1. The lattice structure of SiMg₂O₄ (left) and Fe/SiMg₂O₄/Fe magnetic tunnel junction (right).

There are two key structure parameters for spinel oxides. One is the lattice constant (a) and the other is the oxygen displacement parameter (u).¹⁵ The fcc lattice is used to relax a and u at the same time. The relaxed structures are listed in Table I, which are in good agreement with available experiments¹⁶ and previous calculations.¹⁵

We first examine the symmetry of the real bands near the conduction band minimum (CBM) and the valence band maximum (VBM). The real bands along Λ and Δ directions are shown in Fig. 2. For spinel oxide, the bands have C_{2v} symmetry along [001] direction. There are four different bands: $\tilde{\Delta}_1$, $\tilde{\Delta}_2$, and the doubly degenerate $\tilde{\Delta}_3$ and $\tilde{\Delta}_4$. The CBM of all four spinel oxides have the $\tilde{\Delta}_1$ symmetry. But the band symmetries near VBM are different. For MgAl₂O₄ and ZnAl₂O₄, the VBM have the $\tilde{\Delta}_1$ and $\tilde{\Delta}_3(\tilde{\Delta}_4)$ symmetries, while for SiMg₂O₄ and SiZn₂O₄ the VBM have $\tilde{\Delta}_3(\tilde{\Delta}_4)$ and $\tilde{\Delta}_2$ symmetries. However, for SiMg₂O₄ and SiZn₂O₄, near the VBM there are $\tilde{\Delta}_1$ bands. All have a direct band gap at the Γ point. The calculated band gaps are 5.84, 4.53, 5.17, and 2.81 eV for MgAl₂O₄, ZnAl₂O₄, SiMg₂O₄, and SiZn₂O₄, respectively, in good agreement with previous results.^{21,22}

The complex bands along [001] direction are calculated by using a tetragonal lattice. As shown in Figs. 3(a)–3(c), for MgAl₂O₄, ZnAl₂O₄, and SiMg₂O₄, the pure imaginary bands closest to the real axis have free-electron-like dispersions. By looking at the symmetry of the real bands, we can verify that these imaginary bands have the $\tilde{\Delta}_1$ symmetry. Within the band gap, the complex band dispersion can be fitted by³

$$\frac{1}{k^2(E)} = \frac{\hbar^2(E_c - E_v)}{2m^*(E - E_v)(E_c - E)}, \quad (1)$$

where the E_v and E_c are the valence and conduction band edges and m^* is the effective mass. For MgAl₂O₄, ZnAl₂O₄, and SiMg₂O₄, the $\tilde{\Delta}_1$ band can be fitted accurately with Eq.

TABLE I. The relaxed lattice constant and oxygen displacement parameter compared with available experimental value and FLAPW calculation results by Wei *et al.*¹⁵ Last column lists the lattice mismatch between the spinel and the bcc-Fe ($a = 2.865$ Å).

| Spinel | a (Å) | a_{exp} (Å) | a (Å) ^a | u | u_{exp} | u ^a | Mismatch (%) |
|----------------------------------|---------|----------------------|----------------------|-------|------------------|------------------|--------------|
| MgAl ₂ O ₄ | 8.054 | 8.083 | 8.072 | 0.390 | 0.387 | 0.389 | 0.25 |
| ZnAl ₂ O ₄ | 8.060 | 8.086 | 8.073 | 0.390 | 0.389 | 0.390 | 0.21 |
| SiMg ₂ O ₄ | 8.041 | 8.076 | 8.039 | 0.369 | ... | 0.369 | 0.33 |
| SiZn ₂ O ₄ | 8.072 | ... | 8.083 | 0.369 | ... | 0.368 | 0.25 |

^aReference 15.

(1). The fitted effective masses are 0.422, 0.408, and 0.418, respectively. For SiZn₂O₄ as is shown in Fig. 3(d), the $\tilde{\Delta}_1$ the top of the pure imaginary bands in the gap is connected to the real $\tilde{\Delta}_1$ conduction band and its bottom is connected to the $\tilde{\Delta}_1$ complex band (as the dash line shown in Fig. 3(d)). This is similar to Kotoite Mg₃B₂O₆.²³

The band symmetry and the corresponding orbital composition of bcc-Fe and spinel oxides along [001] direction are listed in Table II. The bcc Fe electrode have four different bands along [001] direction. There are Δ_1 , Δ_2 , Δ_2' , and Δ_5 . By considering the symmetry, the electrons that come from the electrodes tunneling into spinel will transform according to different symmetry in spinel. The Δ_1 and Δ_2' band of Fe will transform as $\tilde{\Delta}_1$ in spinel. The Δ_5 band of Fe will transform as degenerating $\tilde{\Delta}_3(\tilde{\Delta}_4)$ and the Δ_2 band of Fe will transform as $\tilde{\Delta}_2$ in spinel. Besides the band symmetry of tunneling electrons, the orbital composition of the bands is also crucial for the transmission. The Δ_2' band of Fe comprises of d_{xy} orbital, and it matches to the $\tilde{\Delta}_1$ band in spinel with $d_{x^2-y^2}$ orbital.

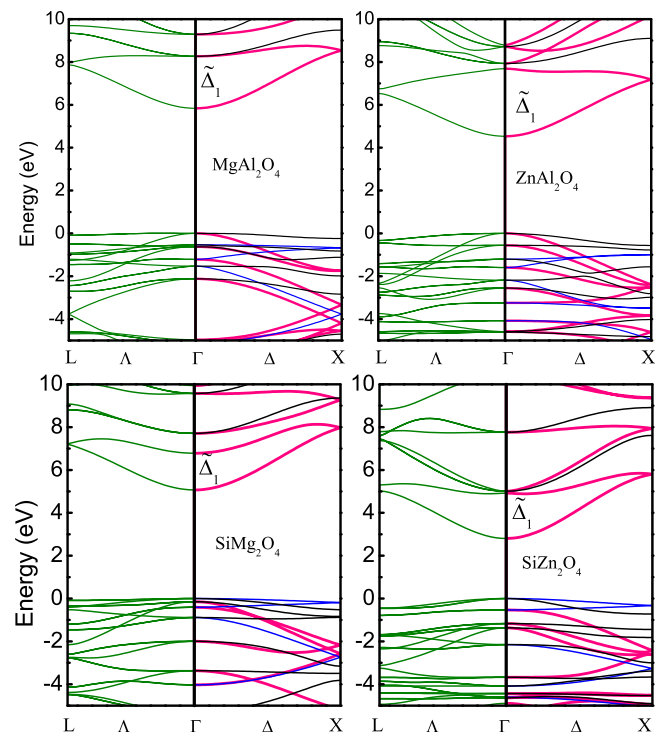


FIG. 2. The real bands of four spinel oxides along Λ and Δ directions in fcc lattice. For the Γ -H direction, there are $\tilde{\Delta}_1$ (pink line), $\tilde{\Delta}_2$ (blue line), and degenerating $\tilde{\Delta}_3$ and $\tilde{\Delta}_4$ (black line).

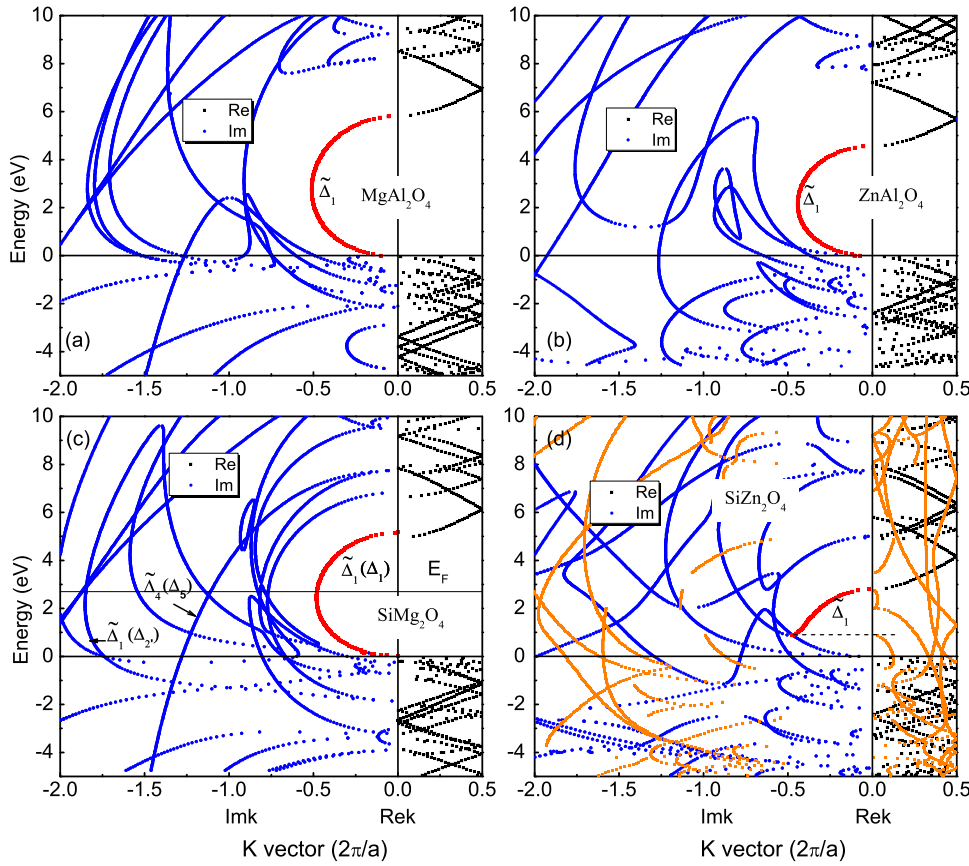


FIG. 3. Real (black), imaginary (blue), and complex (orange for SiZn_2O_4) bands along [001] direction for (a) MgAl_2O_4 , (b) ZnAl_2O_4 , (c) SiMg_2O_4 (symmetry of the matched majority bands in bcc-Fe are shown in parentheses), (d) SiZn_2O_4 . The $\tilde{\Delta}_1$ imaginary bands are shown in red. Dashed line in (d) indicates the bottom of the $\tilde{\Delta}_1$ imaginary band where it is connected to the top of a complex $\tilde{\Delta}_1$ band.

To further analyze the spin-filter effect, the transport properties of $\text{Fe}/\text{SiMg}_2\text{O}_4/\text{Fe}$ MTJ are calculated. The MTJ structure adopted is shown in Fig. 1(b). To simplify the calculation task, only one unit cell of SiMg_2O_4 is used as tunnel barrier, and $100 \times 100k_{\parallel}$ points in two dimensional Brillouin zone (2D BZ) are used for transmission calculation. Majority spin and minority spin transmission for the parallel moment alignment are shown in Figs. 4(a) and 4(c). For majority electron large transmission is found in 2D BZ around the $\bar{\Gamma}$ point. The sharp spikes in the transmission for both parallel and anti-parallel configurations may be due to interface resonance states.³ They will be diminished with thicker barriers or in real MTJs.²⁴ In order to identify which Bloch state is dominated at $\bar{\Gamma}$ point, the scattering Bloch states density is calculated. The scattering Bloch states density reflects how different Bloch states transmit through the junction. The scattering Bloch states charge density as a function of z direction is calculated by integrating the tunneling Bloch states density in XY plane as implemented in PWCOND of

Quantum Espresso package.¹⁹ As shown in Fig. 4(b), the majority Δ_1 state in Fe has the largest transmission at the $\bar{\Gamma}$ point, the Δ_5 state shows a faster decay in the barrier, and the $\Delta_{2'}$ state has the most rapid decay. As it is shown in Table II, although the $\Delta_{2'}$ in Fe also transform as $\tilde{\Delta}_1$ in spinel, its orbital composition is d_{xy} , so it has the smallest transmission probability. The decay rate can be estimated by scaling the scattering density of states in Fig. 4(b) to e^{-2kd} , from which we find the values of k as 0.54, 1.01, and 1.79 (in $2\pi/a$) for majority $\Delta_1, \Delta_5, \Delta_{2'}$ states, respectively. For minority Δ_2 state, k is estimated to be 1.91. These values are in excellent agreement with the imaginary band wave vectors listed in Table II.

Besides the spinel oxides, we point out that along the [001] direction most of the Zinc-blende semiconductors (GaAs, ZnSe (Ref. 17)) and rocksalt-type insulators (MgO, NaCl, MgB_2O_6 (Ref. 23)) all have similar Δ_1 spin-filter effect thus considerable magneto-resistance can be expected in MTJs using these materials as tunnel barriers. Both of the CBM and VBM in these materials have the Δ_1 symmetry. For example, for most of the Zinc-blend semiconductors and rocksalt semiconductors at $\bar{\Gamma}$, their CBM has Γ_1 symmetry and their VBM have Γ_{15} symmetry.^{25–28} Thus they will be connected by a purely imaginary band with Δ_1 symmetry. There are exceptions. For example, some perovskite-type compounds, the band symmetry of CBM at $\bar{\Gamma}$ is $\Gamma_{25'}$ and the VBM is Γ_{15} . The complex band connecting these points across the gap will have the Δ_5 symmetry.^{29–31} Because of their better lattice mismatch, the spinel oxides may be the best candidate barrier materials for improved performance of MTJs.

TABLE II. Fe and spinel band symmetries. The orbital composition is listed in parenthesis. The last column shows the corresponding imaginary band for SiMg_2O_4 at the Fermi energy of $\text{Fe}/\text{SiMg}_2\text{O}_4/\text{Fe}$ -MTJ.

| Fe | Rotate 45° | Spinel | Imk(2π/a) |
|--------------------------------|---------------|---|-----------|
| $\Delta_1(sp_zd_{z^2})$ | Δ_1 | $\tilde{\Delta}_1(sp_zd_{z^2})$ | 0.47 |
| $\Delta_2(d_{x^2-y^2})$ | $\Delta_{2'}$ | $\tilde{\Delta}_2(d_{xy})$ | 1.86 |
| $\Delta_{2'}(d_{xy})$ | Δ_2 | $\tilde{\Delta}_1(d_{x^2-y^2})$ | 1.84 |
| $\Delta_5(p_xp_yd_{zx}d_{yz})$ | Δ_5 | $\tilde{\Delta}_3(p_xd_{zx}, \tilde{\Delta}_4(p_yd_{yz})$ | 1.04 |

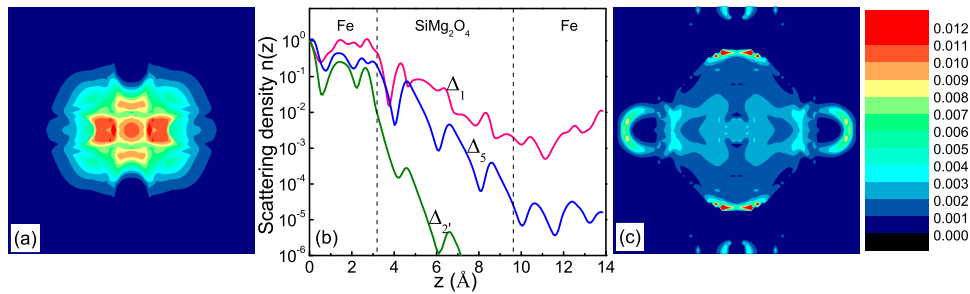


FIG. 4. Fe/SiMg₂O₄/Fe MTJ with parallel moments: (a) The majority spin transmission in 2D BZ. (b) Scattering Bloch states density along z axis at $\bar{\Gamma}$ point for majority spin. (c) The minority spin transmission in 2D BZ.

We thank Dr. D. A. Stewart and Dr. A. Smogunov for discussion. This project was supported by the State Key Project of Fundamental Research of Ministry of Science and Technology [MOST, No. 2010CB934400] National Natural Science Foundation [NSFC, Grant Nos. 10934099, 50928101 and 51021061], and International Collaborative Research Program between NSFC and ANR of France [Grant No. F040803]. A portion of this research was conducted at the CNMS, sponsored at ORNL by the Division of Scientific User Facilities, U.S. Department of Energy.

¹T. Miyazaki and N. Tezuka, *J. Magn. Magn. Mater.* **139**, L231 (1995).

²J. S. Moodera, L. R. Kinder, T. M. Wong, and R. Meservey, *Phys. Rev. Lett.* **74**, 3273 (1995).

³W. H. Butler, X.-G. Zhang, T. C. Schulthess, and J. M. MacLaren, *Phys. Rev. B* **63**, 054416 (2001).

⁴X.-G. Zhang and W. H. Butler, *Phys. Rev. B* **70**, 172407 (2004).

⁵Y. Wang, X. F. Han, and X.-G. Zhang, *Appl. Phys. Lett.* **93**, 172501 (2008).

⁶Y. Wang, J. Zhang, X.-G. Zhang, H.-P. Cheng, and X. F. Han, *Phys. Rev. B* **82**, 054405 (2010).

⁷J. Zhang, Y. Wang, X.-G. Zhang, and X. F. Han, *Phys. Rev. B* **82**, 134449 (2010).

⁸S. S. P. Parkin, C. Kaiser, A. Panchula, P. M. Rice, B. Hughes, M. Samant, and S.-H. Yang, *Nat. Mater.* **3**, 862 (2004).

⁹S. Yuasa, T. Nagahama, A. Fukushima, Y. Suzuki, and K. Ando, *Nat. Mater.* **3**, 868 (2004).

¹⁰S. Yuasa and D. D. Djayaprawira, *J. Phys. D* **40**, R337 (2007).

¹¹S. Ikeda, J. Hayakawa, Y. Ashizawa, Y. M. Lee, K. Miura, H. Hasegawa, M. Tsunoda, F. Matsukura, and H. Ohno, *Appl. Phys. Lett.* **93**, 082508 (2008).

¹²F. Bonell, S. Andrieu, C. Tiusan, F. Montaigne, E. Snoeck, B. Belhadji, L. Calmels, F. Bertran, P. L. Fvre, and A. Taleb-Ibrahimi, *Phys. Rev. B* **82**, 092405 (2010).

¹³H. Sukegawa, H. Xiu, T. Ohkubo, T. Furubayashi, T. Niizeki, W. Wang, S. Kasai, S. Mitani, K. Inomata, and K. Hono, *Appl. Phys. Lett.* **96**, 212505 (2010).

¹⁴R. Shan, H. Sukegawa, W. Wang, M. Kodzuka, T. Furubayashi, T. Ohkubo, S. Mitani, K. Inomata, and K. Hono, *Phys. Rev. Lett.* **102**, 246601 (2009).

¹⁵S.-H. Wei and S. B. Zhang, *Phys. Rev. B* **63**, 045112 (2001).

¹⁶R. J. Hill, J. R. Craig, and G. V. Gibbs, *Phys. Chem. Miner.* **4**, 317 (1979).

¹⁷Ph. Mavropoulos, N. Papanikolaou, and P. H. Dederichs, *Phys. Rev. Lett.* **85**, 1088 (2000).

¹⁸P. Giannozzi, S. Baroni, N. Bonini, *et al.*, *J. Phys.: Condens. Matter* **21**, 395502 (2009).

¹⁹A. Smogunov, A. D. Corso, and E. Tosatti, *Phys. Rev. B* **70**, 045417 (2004).

²⁰J. Monkhurst and J. D. Pack, *Phys. Rev. B* **13**, 5188 (1976).

²¹S. K. Sampath, D. G. Kanhere, and R. Pandey, *J. Phys.: Condens. Matter* **11**, 3635 (1999).

²²A. Bouhemadou and R. Khenata, *Modell. Simul. Mater. Sci. Eng.* **15**, 787 (2007).

²³D. A. Stewart, *Nano Lett.* **10**, 263 (2010).

²⁴K. D. Belashchenko, J. Veleev, and E. Y. Tsymlal, *Phys. Rev. B* **72**, 140404(R) (2005).

²⁵S. T. Pantelides and W. Harrison, *Phys. Rev. B* **11**, 3006 (1975).

²⁶C. S. Wang and B. M. Klein, *Phys. Rev. B* **24**, 3393 (1981).

²⁷S. T. Pantelides, *Phys. Rev. B* **11**, 5082 (1975).

²⁸R. Pandey, J. E. Jaffe, and A. B. Kunz, *Phys. Rev. B* **43**, 9228 (1991).

²⁹L. F. Mattheiss, *Phys. Rev. B* **6**, 4718 (1975).

³⁰J. P. Veleev, C.-G. Duan, K. D. Belashchenko, S. S. Jaswal, and E. Y. Tsymlal, *Phys. Rev. Lett.* **98**, 137201 (2007).

³¹L. F. Mattheiss, *Phys. Rev. B* **5**, 290 (1972).